TÜBİTAK

Turkish Journal of Earth Sciences

http://journals.tubitak.gov.tr/earth/

Research Article

Turkish J Earth Sci
(2014) 23: 559-574
© TÜBİTAK
doi:10.3906/yer-1401-3

A microscopic approach to the pedogenic formation of palygorskite associated with Quaternary calcretes of the Adana area, southern Turkey

Meryem YEŞİLOT KAPLAN[1], Muhsin EREN[2,*], Selahattin KADİR[3], Selim KAPUR[4], Jennifer HUGGETT[5]

[1]Department of Petroleum and Natural Gas Engineering, Mustafa Kemal University, İskenderun, Hatay, Turkey
[2]Department of Geological Engineering, Mersin University, Mersin, Turkey
[3]Department of Geological Engineering, Eskişehir Osmangazi University, Eskişehir, Turkey
[4]Departments of Soil Science and Archeometry, Çukurova University, Adana, Turkey
[5]Department of Earth Sciences, Natural History Museum, London, UK

Received: 03.01.2014 • **Accepted:** 06.08.2014 • **Published Online:** 01.09.2014 • **Printed:** 30.09.2014

Abstract: Quaternary calcretes in the Adana area (southern Turkey) are widespread and occur in a variety of forms such as nodular, columnar/tubular, fracture-infill, laminated hardpan, and conglomeratic crusts. Palygorskite associated with calcrete nodules, tubes, and fracture-infills in the columnar horizon and adjacent host-rock mudstones suggests a cogenetic formation. The β-fabric (biogenic) constituents and stable isotope values of calcretes support a pedogenic origin for calcretes and also palygorskite. Extensions of palygorskite fibre and fibre bundles from euhedral to subhedral calcite crystals in calcretes and from smectite flakes in adjacent host-rock mudstone suggest an authigenic origin related to calcretisation in which precipitation and dissolution/precipitation are the main processes for palygorskite formation, respectively. The presence of palygorskite in subspherical aggregates containing calcite crystals, and with smectitic clay coatings around the palygorskite aggregate, similarly suggests a relationship of pedogenic evolution between the 2 clays. Palygorskite precipitated in a vadose zone from strongly evaporated alkaline water, rich in Si and Mg and low in Al and Fe, at elevated temperatures and at an advanced stage of calcrete formation. Development of palygorskite mainly on relict calcite crystals indicates its formation during or shortly following calcite formation in calcretes. Palygorskite precipitation on relative large crystal surfaces has resulted in encrusted and platy fan-like crystal morphologies, whereas its nucleation on the crystal edge relief triggers fibre-like morphologies from crystal edges.

Key words: Authigenesis, calcrete, geochemistry, mineralogy, palygorskite, pedogenesis, Quaternary, smectite

1. Introduction

Palygorskite [$Si_8Mg_2Al_2O_{20}(OH)_2(OH_2)_4.4H_2O$] is a common phyllosilicate known from marine and continental sediments, soils, and hydrothermally affected rocks (Singer, 1989; Suárez et al., 1994; Wang et al., 2009). Its occurrence is also reported from calcretes as a minor component (Wright and Tucker, 1991; Verrecchia and Le Coustumer, 1996; Eren et al., 2008; Kaplan et al., 2013). Palygorskite studies are frequent in the literature (e.g., Singer and Norrish, 1974; Elprince et al., 1979; Verrecchia and Le Coustumer, 1996; Krekeler et al., 2005; Kadir and Eren, 2008; Garcia-Romero and Suárez, 2010; Galán and Pozo, 2011; Yalçın and Bozkaya, 2011; Yeniyol, 2012), and some stress the widespread pedogenic occurrence of palygorskite in contemporary arid and semiarid climatic zones of the globe (e.g., Singer and Norrish, 1974; Elprince et al., 1979; Hassouba and Shaw, 1980; Botha and Hughes, 1992; Hillier and Pharande, 2008). Verrecchia and Le Coustumer (1996) and Yalçın and Bozkaya (2011) have compiled and summarised palygorskite studies in the world and also in Turkey, respectively. Nonetheless, despite the limited area covered, i.e. confined to the boundaries of Turkey, the studies conducted by Yılmaz (1999), Kapur et al. (1987, 1990, 1993, 2000), Kadir and Eren (2008), Kadir et al. (2010), Eren et al. (2004, 2008), Kaplan et al. (2013), Küçükuysal et al. (2014). and Kadir et al. (2014) of pedogenic palygorskite and calcretes have contributed to the understanding of the major components and genesis as well as the mineralogical and micromorphological aspects of palygorskite associated with calcretes. Consequently, this study focuses on the detailed microscopic determination of palygorskite in calcretes and smectitic host rocks based on bulk and polished thin sections, microchemistry, and pedogenic origin. This research will provide new data to help to explain the physicochemical condition of pedogenesis and the related palaeoclimatic conditions in the Eastern Mediterranean Basin.

* Correspondence: m_eren@yahoo.com

2. Materials and methods

Eighty-four samples of calcrete and adjacent host rocks were analysed by X-ray powder diffractometry (XRD) to determine their mineralogical composition and distribution of palygorskite in the samples. XRD analyses were performed using CuK radiation at a scanning speed of 2° 2/min at the Turkish Petroleum Corporation (TPAO, Ankara, Turkey). Clay minerals were identified via separated clay fractions (<2 μm) by sedimentation, followed by centrifugation of the suspension, after overnight dispersion in distilled water. The clay particles were dispersed by ultrasonic vibration for about 15 min. Three oriented specimens of the <2 μm fraction were prepared from each sample, then air-dried, ethylene-glycol-solvated at 60 °C for 2 h, and thermally treated at 550 °C for 2 h. Semiquantitative relative abundances of rock-forming minerals were obtained using the method of Brindley (1980), and the relative abundances of clay-mineral fractions were determined using their basal reflections and the intensity factors of Moore and Reynolds (1989). Energy dispersive X-ray (EDX) analyses of single points were obtained from carbon-coated polished thin sections of selected samples using a Zeiss EVO scanning electron microscope with an Oxford Instruments ISIS X-ray analytical facility. Operating conditions were a 2 μA beam current at 15 kV accelerating voltage. Detection limits vary according to the element being detected and the matrix in which it is contained; for these samples, detection limits are 0.2% for Mg, Ca, and K and 0.4%–0.6% for Al, Si, P, Mn, Ti, and Fe. Calibration using a cobalt standard was performed prior to analysis, and the beam current was monitored during analysis. Only analyses with analytical totals in the correct range for palygorskite were retained. The structural formulae of palygorskite and smectite were calculated from microchemical analysis based on 21 and 22 atoms, respectively.

Scanning electron microscopy (SEM) studies were performed at Eskişehir Osmangazi University (Turkey) using a JEOL JSM 84A instrument equipped with an EDX detector. Representative clay-rich bulk samples were prepared for the SEM studies by adhering the fresh, broken surface of each rock sample onto an aluminium sample holder using double-sided tape. Samples were coated with thin films (~350 Å) of gold using a Giko model ion coater. Transmission electron microscopy (TEM) studies were carried out at Anadolu University (Turkey) using a JEOL JEM-21007 instrument. The clay particles for TEM studies were dispersed by an ultrasonic ethanol bath for about 30 min, and a single drop of each clay suspension was placed on carbon-coated copper grids and dried at room temperature. The separated clay fractions were analysed via infrared spectrometry (IR) (PerkinElmer 100 FTIR spectrometer) in order to determine their mineralogical characteristics.

3. Geological setting

The study area is located in the northern part of the Adana Basin, which is one of the major Neogene basins in the Tauride orogenic belt (Figure 1; Yalçın and Görür, 1983; Eren et al., 2007). Tertiary and Quaternary units are widespread and unconformably overlie Palaeozoic and Mesozoic basement rocks in the Adana Basin

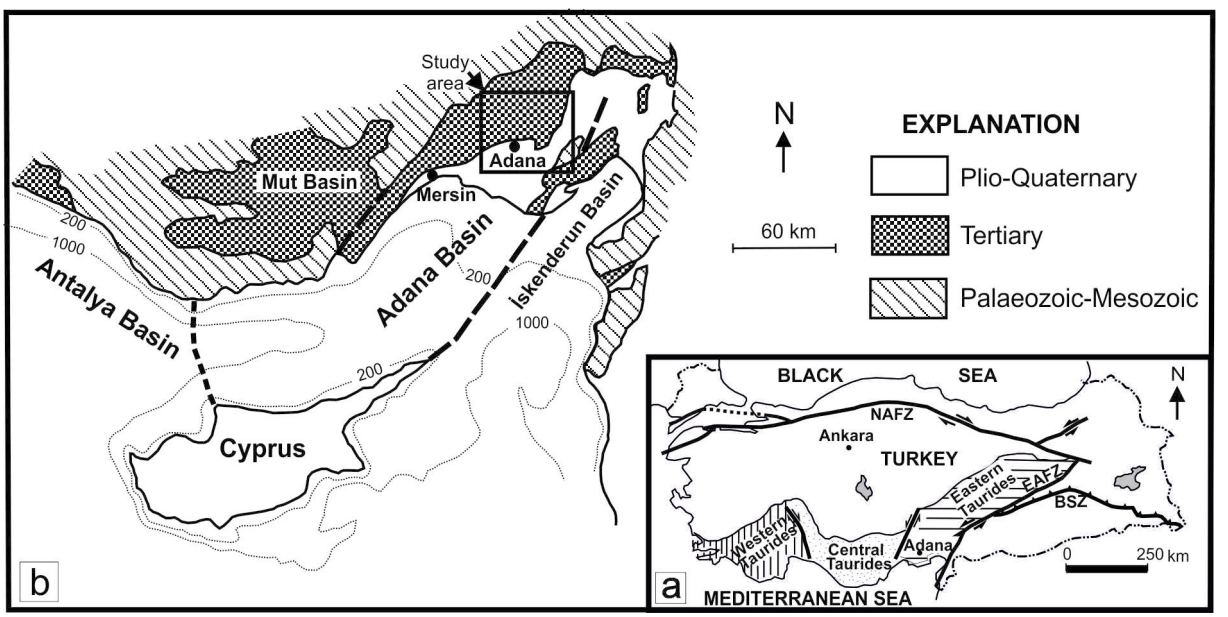

Figure 1. (a) Schematic map of Tauride Orogenic Belt and its subdivisions (Eren et al., 2007). NAFZ: North Anatolian Fault Zone, EAFZ: East Anatolian Fault Zone. **(b)** Location map of the study area in the Adana Basin.

(Yalçın and Görür, 1983; Yetiş, 1988; Yetiş et al., 1995; Gürbüz, 1999). The Kuzgun (Tortonian) and Handere (Messinian–Pliocene) formations and the Quaternary units widely outcrop in the area (Figures 2 and 3). The Kuzgun Formation (Tortonian) consists of shallow marine to nonmarine sandstones and mudstones. The Handere Formation comprises mainly mudstones and also conglomerates and sandstones of shallow marine, lagoonal, and fluvial environments (Yetiş, 1988; Yetiş et al., 1995; Gürbüz, 1999). Quaternary units include alluvial terraces, patches of lagoonal remnants, hardpan calcretes, and recent alluvium.

Calcretes are widespread on and/or within the Handere Formation in the study area. Some calcrete occurrences also appear in Pleistocene alluvial terraces (Kapur et al., 1993; Kaplan et al., 2013). An Early Holocene-Pleistocene age was reported for calcretisation by Atalay (1996), Kapur et al. (1987, 1990, 2000), and Eren (2011). Atalay (1996) and Özer et al. (1989) also determined similar ages of 250 to 782 ka BP by electron spin resonance and thermoluminescence dating for the calcretes.

Calcretes occur in a variety of forms such as nodular, columnar/tubular, fracture-infilled, laminated hardpans, and conglomeratic crusts in the Adana area. In general, calcrete profiles are characterised by a hard laminated crust (hardpan) at the upper part and nodules and/or tubes at the lower parts as the column horizon (Figures 4a–4f) (Kapur et al., 1987, 1990; Kaplan et al., 2013). Nontectonic fracture fillings are rarely associated with the columnar horizons determined in calcrete sections. The calcrete hardpan occupies large areas as wavy capping on the slightly undulating terrain and covers the lithologically different beds of the Handere Formation, in particular the red mudstones (Figure 4b). The hardpan is a typically cream coloured, evenly discontinuous laminated, indurated, wavy horizon rich in calcium carbonate with an average thickness of 0.5 to 2.0 m. The carbonate crust represents a sharp upper surface, generally covered by soil with a variable depth and a lower contact, grading into the columnar horizon (Figure 4b) with a depth ranging from 0.5 to 3 m, up to 10 m. Calcrete nodules and tubes/columns are common especially in the red mudstones of the Handere Formation with associated nontectonic fracture infills. The nodules, tubes, and fracture-infills are semiindurated, white-coloured, and finely crystalline calcite (Figures 4b–4d). The nodules (2 to 35 cm) are crudely spherical to irregular or ellipsoid in shape and often isolated (Figure 4c) and locally in coalesced arrangement.

4.Results

4.1. XRD analyses

The results of XRD analyses revealed that palygorskite is associated with calcite in the calcretes, except in the hard laminated crust (hardpan), where it is a very minor component (Table 1). Smectite is dominant in the mudstone of the host-rock, followed by calcite, quartz, feldspar, and illite. Palygorskite was determined via its ideal diagnostic sharp reflection at 10.5 Å, which is not affected by ethylene-glycol solvation due to its nonexpandable character. This reflection collapsed to 10.2 Å following heating to 550 °C for 2 h (Figure 5), whereas the mudstone smectite basal reflection at 14.81 Å expanded to 15.71 Å upon ethylene-glycol treatment and collapsed to 10 Å upon heating to 350 °C. Illite was determined by reflections at 10 and 5.01 Å where the latter was overlapped by basal reflection of palygorskite. Calcite was determined by sharp reflections at 3.04, 4.86, 2.50, and 2.29 Å.

4.2. Infrared spectra

The IR spectra for a representative palygorskite-dominated sample is given in Figure 6. The occurrences of the bands at 3618, 1427, 1032, 875, 798, 518, and 471 cm^{-1} were attributed to the presence of palygorskite. Bands at 3618 cm^{-1} correspond to the stretching vibration of OH coordinated to Al and Fe (AlAlOH, AlFeOH) in the octahedral site of palygorskite (Frost et al., 2001; Suárez and García-Romero, 2006). The band at 875 cm^{-1} is characteristic of the AlMgOH. The band at 1644 cm^{-1} corresponds to the vibration of adsorbed and zeolitic water (Farmer, 1974; Suárez and García-Romero, 2006). The 1032, 798, 518, and 471 cm^{-1} bands are characteristic of the Si-O stretching vibrations in the tetrahedral site (Farmer, 1974).

4.3. SEM and TEM studies

Representative palygorskite-dominated samples were selected for SEM-EDX analyses. In SEM images, palygorskite is associated with euhedral to subhedral calcite crystals in calcrete nodules and tubes (Figures 7a–7e) and smectite flakes (Figures 7f–7i) in the mudstones of the calcrete host-rock. Palygorskite is fibrous and appears as a wedge (Figures 7g and 7h) extending over/between calcite crystals in calcretes (Figures 7a and 7b) or smectite flakes in mudstones (Figures 7g and 7h). It also covers and bridges calcite crystals (Figures 7c–7e) and has interwoven mats (Figure 7f) and platy fan-like (Figure 7i) features. The platy fan-like palygorskite bundles of palygorskite fibres are club-shaped and often exhibit narrow and sharp edges (Figure 7i). The elongated platy fan-like palygorskite and the interwoven mat-like fibres both have a length of about 8–20 μm and a thickness of less than 1 μm (Figures 7a–7g). Palygorskite fibres associated with calcite have a length of less than 8 μm with a width of less than 1 μm (Figure 7h–7j), whereas the palygorskite fibres edging the smectite plates in mudstone are finer (1–4 μm in length) (Figure 7k).

TEM studies showed that palygorskite particles occur as fibres, fibre bundles, and fan- and bridge-like forms

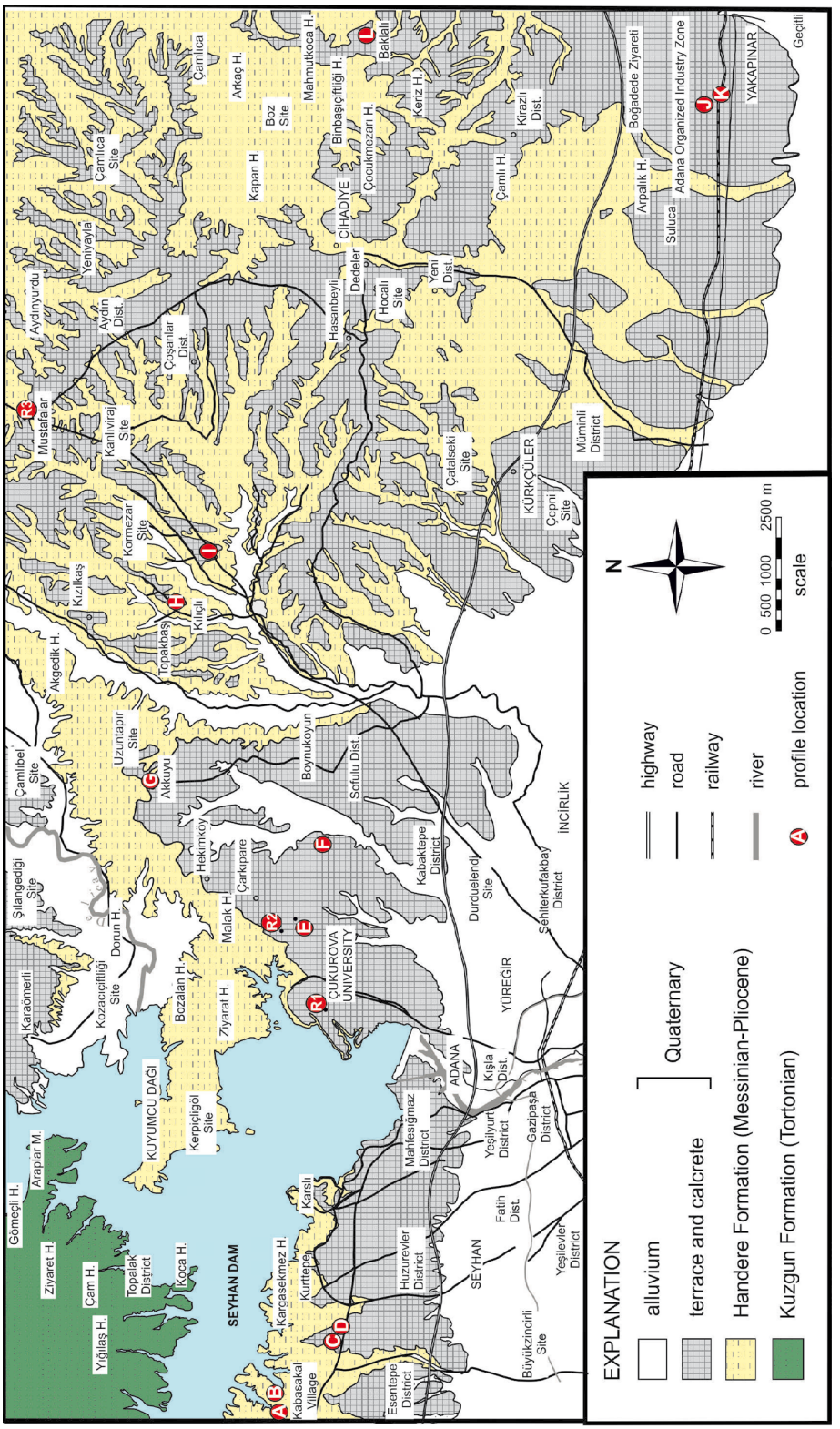

Figure 2. Generalised geological map of the study area (modified from Yetiş, 1988).

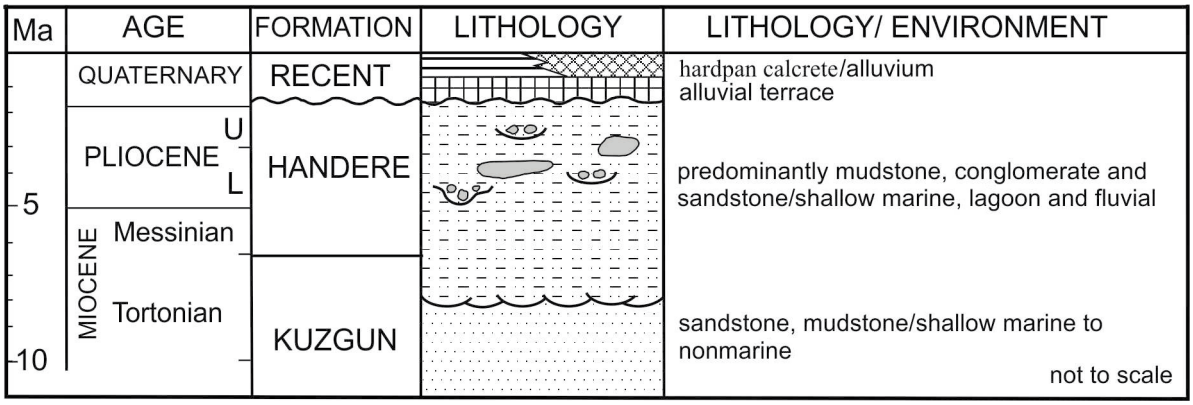

Figure 3. Simplified stratigraphic column of the study area (modified from Gürbüz, 1999).

(Figures 8a–8f). Palygorskite fibres and fibre bundles are the most common forms extending from calcite and smectite crystals. Some palygorskite fibres in mesh-like forms curve around micropores that were previously filled by impurities, later removed during the purification processes (Figure 8c). The bridge-like forms of palygorskite between calcite crystals (Figure 8d) consist of fibre bundles in which some fibres are bent. Individual palygorskite fibres are thin and have a high width/thickness ratio. The lengths of palygorskite fibres range from 300 to 600 nm, with diameters from 15 to 70 nm. Sharp outlines of the individual fibres suggest moderate to high crystallinity and its in situ formation rather than transportation. Fan-like forms of palygorskite resemble dissolution/precipitation from smectite (Figure 8d–8f).

4.4. Chemistry of palygorskite and smectite

Chemical compositions of palygorskite and smectite single points were obtained from EDS X-ray samples B-2, K-8, MY-3, YY-1, and YY-10 (Table 2). Only sample YY-10 contains clearly defined subspherical aggregates of palygorskite large enough to analyse (Figure 9a). Small amounts of K were determined in this sample, indicating that the clayey rim (around the palygorskite aggregate)/ clay coating may contain mixed-layer smectite-illite. The clay coating was most likely developed/deposited around the aggregate surfaces following illuviation during pedogenesis. In all other samples (e.g., B-2, Figure 9b) the clays appear to be mixed on a scale too fine to resolve using the Zeiss EVO SEM. All samples contain particles of calcite <5 μm throughout the clay, and similarly sized particles of Ti oxide are also widespread. Inevitably, some analyses include a contribution from the calcite and Ti oxide minerals. To eliminate this contamination from the calculated formulae, only those analyses without Ti contamination and containing <0.5% K, >4% Mg, and <0.5 % Ca were used to calculate the palygorskite formula of $(Si_{7.55}Al_{0.45})(Al_{1.78}Fe_{0.53}Mg_{1.60})(Ca_{0.08}K_{0.12})$, and only analyses without Ti contamination and containing <4% Mg and <2 % Ca were used to calculate the smectite formula of $(Si_{7.71}Al_{0.29})(Al_{2.26}Fe_{0.75}Mg_{0.96})(Ca_{0.23}K_{0.36})$. In addition to Mg, significant amounts of Fe and Al are present in the palygorskite and smectite octahedral sites, while Al occurs in tetrahedral sites of both minerals. The Ca and K were deemed to be exchangeable interlayer cations. The smectite may be classified as montmorillonite. The octahedral sites of palygorskite are occupied by Al+Fe > Mg and Al > Fe; therefore, the mineral can be defined as an aluminic palygorskite (Garcia-Romero and Suárez, 2010). The composition of the smectite sample is similar to that of montmorillonite from Kakkonda, Japan (Inoue et al., 2004), though slightly more Fe-rich.

5. Discussion

Both XRD and SEM/TEM studies reveal a close association of palygorskite with calcretes and their host-rock mudstone. The mudstone is predominantly smectite of detrital origin. Palygorskite frequently occurs within calcrete nodules, tubes, and fracture-infills and adjacent host-rock mudstone in the calcrete profile/section. The abundance of β-fabric (biogenic) constituents in the calcrete hardpan (Kaplan et al., 2013) such as rhizoliths, calcite needles, and calcified filaments suggests that palygorskite development likely took place within a biogenically active zone of a soil profile. In addition, the presence of circumgranular and desiccation cracks, alveolar textures, vadose pisolites, and vadose silts in the hardpan suggests the formation of palygorskite in the vadose environment (Hassouba and Shaw, 1980; Eren et al., 2004, 2008; Kaplan et al., 2013). The vadose environment is also supported by the presence of the clay coatings as determined by Kapur et al. (1987) and Kaplan et al. (2013) present within the calcrete nodules and tubes, and the development of palygorskite as sheet-like fibre bundles (Figure 7b) and fibre bridges as meniscus cement between the calcite crystals (Figures 7d, 7e, and 8d). The pedogenic origin of palygorskite is inferred from

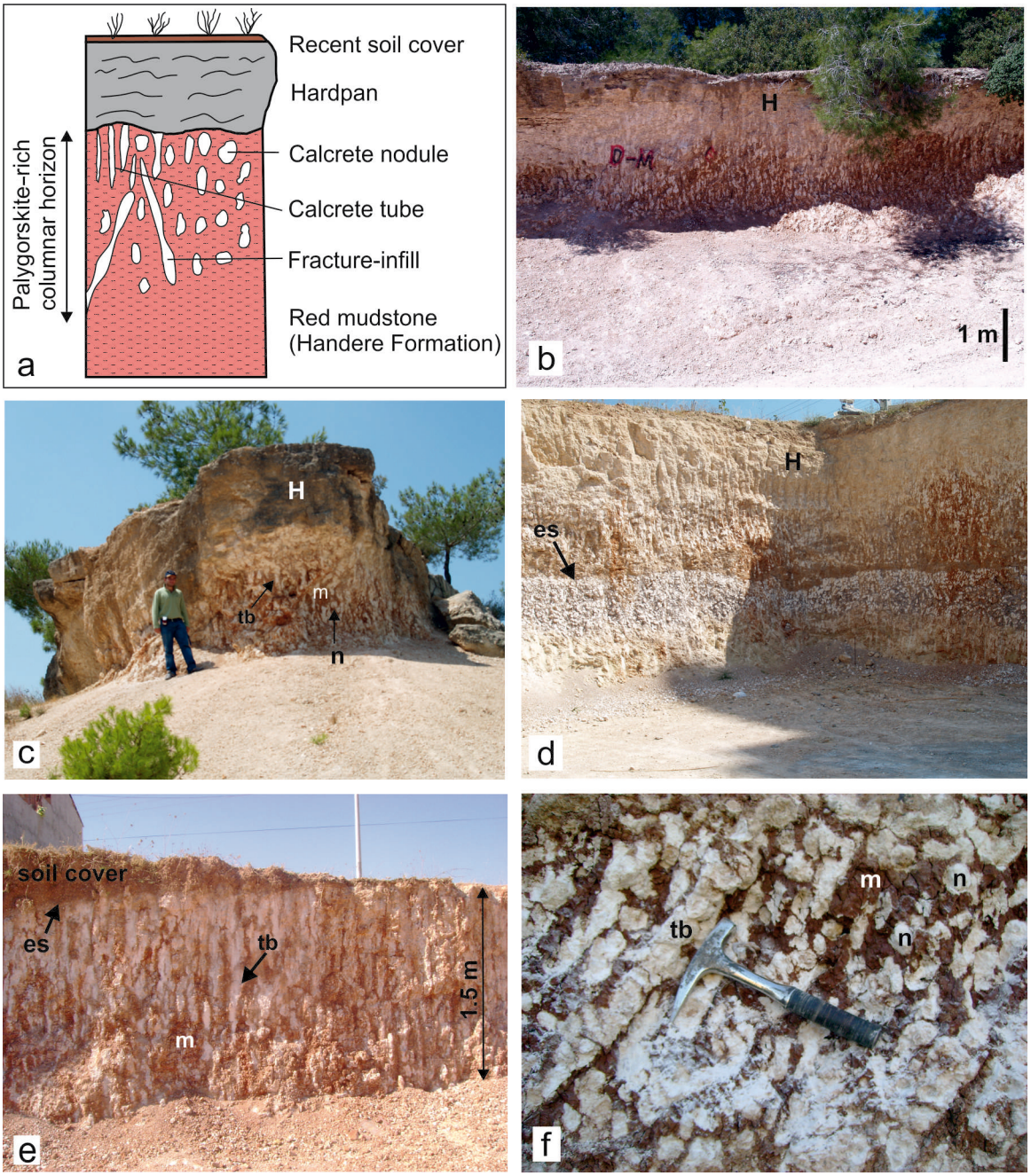

Figure 4. (a) Schematic presentation of most common calcrete profile and field photographs: **(b–d)** well-developed calcrete profiles from H, I, and C locations, showing the hard laminated crust (hardpan; H) at upper part and nodular (n)-tubular (tb) horizon (columnar horizon; white mottling) in red mudstones of the Handere Formation at lower part. In **(d)**, calcrete development was interrupted by palaeoerosion (es: erosional surface); **(e)** Sarıçam profile (location F) showing calcrete tubes (tb) in the red mudstones of the Handere Formation, which were truncated by contemporary erosion (es: erosional surface) and covered by recent soil; **(f)** close views of calcrete nodules (n) and tubes (tb) (white mottling) in the red mudstones (Handere Formation, location E).

the abundance of biological components in the hardpan calcrete and from stable isotope values of calcretes provided by Kaplan et al. (2013). The $\delta^{18}O$ and $\delta^{13}C$ values of calcite in calcrete samples range from –3.76‰ to –5.74‰ (mean: –4.40‰) and from –7.71‰ to –10.01‰ (mean: –8.55‰) PDB, respectively (Kaplan et al., 2013). The $\delta^{18}O$ values of calcretes are consistent with precipitation from meteoric water (James and Choquette, 1984; Purvis and Wright,

Table 1. Semiquantitative mineralogical compositions of the selected calcrete and host-rock mudstone samples.

Sample no.	Location	Calcite	Quartz	Feldspar	Palygorskite	Smectite	Illite	Chlorite	Amphibole	Gypsum
Mudstone										
KA-3	A	++	+	ac	+	++	ac	ac		
O-5	C	+	+		+	++	ac	ac		
O-8	C	+	+	ac	++	+	ac	ac		
YY-1	D	+	+	ac	++	+	ac	ac		
YY-10	D	+	+	ac	++	+	ac	ac		
TO-2	E	+	+	ac	+	++	ac	ac		
SB-2	F	+	+	ac	++	+	ac	ac		
K-8	H	++	+	ac	+	++	ac	ac		
SA-4	I	++	ac	ac	++	++	ac	ac		
Y-1	J	++	+	ac	ac	++	ac	ac		
M-1	K	++	+	ac	++	++	ac	ac		
B-2	L	++	+	ac	+	++	ac	ac		
C-5	R1	++	+	ac	ac	+	ac	ac	ac	ac
S-4	R2	+	+	ac	ac	+++	ac	ac		
IMY-3	R3	++	+	ac	+	++	ac	ac		
Calcrete nodule and tube										
KA-1	A	+++++	ac	ac	ac					
O-2	C	+++++	ac							
O-3	C	+++++	ac							
O-4	C	+++++								
O-6	C	+++++	ac	ac		ac				
O-7	C	+++++	ac							
YY-3	D	+++++	ac	ac	ac					
YY-4	D	+++++	ac	ac	ac					
YY-7	D	+++++	ac							
YY-8	D	+++++	ac							
YY-9	D	+++++	ac							
TO-1	E	+++++	ac							
AK-1	G	+++++	ac		ac					
K-3	H	+++++	ac							
K-5	H	+++++	ac	ac						
K-6	H	+++++	ac	ac						
K-7	H	+++++	ac							
SA-1	I	+++++	ac			ac				
SA-2	I	+++++								
SA-3	I	+++++	ac							
Y-2	J	+++++	ac							
Y-5	J	+++++	ac							
M-2	K	+++++	ac							
B-1	L	+++++	ac							

Table 1. (Continued).

C-4	R1	+++++	ac	ac		
C-6	R1	+++++	ac			
S-3	R2	+++++	ac			
S-5	R2	+++++				
S-7	R2	+++++	+	ac		
İMY-2	R3	+++++	ac			
Calcrete hardpan						
KA-2	A	+++++	ac			
ÇKK	B	+++++	ac	ac		
O-9	C	+++++	ac			
YY-5	D	+++++	ac			
SB-3	F	+++++	ac			
AK-2	G	+++++	ac		ac	
K-1	H	+++++	ac			
SA-5	I	+++++	ac			
Y-6	J	+++++	ac			
M-3	K	+++++	ac			
M-4	K	+++++	ac			
B-3	L	+++++	ac			
Calcrete fracture-infill						
YY-2	D	+++++	ac		ac	
YY-6	D	+++++	ac		ac	
KCD	H	+++++	ac	ac	ac	

+ : Relative abundance of minerals; ac : accessory.

1991; Strong et al., 1992; Jimenez de Cisneros et al., 1993; Alonso-Zarza and Arenas, 2004; Eren et al., 2004, 2008; Shaaban, 2004; Gong et al., 2005; Kaplan et al., 2013), whereas the $\delta^{13}C$ values reflect a high input of soil-derived CO_2 and are also consistent with a pedogenic origin for the calcrete and associated palygorskite (Cerling, 1984, 1992; Boutton, 1991; Wright and Tucker, 1991; Alonso-Zarza, 1999; Eren et al., 2004, 2008; Bajnoczi et al., 2006; Kaplan et al., 2013).

Palygorskite in sedimentary rocks and soils can be inherited/detrital, formed through transformation of precursor clays (aggradation and degradation) or authigenically (e.g., Millot, 1970; Allen and Hajek, 1989; Galán and Pozo, 2011; Yalçın and Bozkaya, 2011). SEM and TEM determinations reveal development of palygorskite fibres on and between authigenic calcite crystals in calcretes, indicating an authigenic formation of palygorskite. It is proposed that, in this setting, direct precipitation of palygorskite was favoured by the increased Mg/Ca ratio resulting from evaporitic calcite precipitation. Conversely, in the host-rock mudstone adjacent to calcrete nodules and tubes, palygorskite is thought to have formed as a result of replacement of smectite. Etched boundaries are consistent with a dissolution/precipitation mechanism rather than a solid-state transformation involving ionic diffusion (Hower et al., 1976; Altaner and Ylagan, 1997; Dudek et al., 2006). Authigenic formation of palygorskite from both transformation of precursor smectite and direct precipitation from soil water with an increase of Mg, Al ± Fe, and Si values has been previously reported by Inglès and Anadón (1991), Chahi et al. (1993), Rodas et al. (1994), Sanchez and Galán (1995), Sárez et al. (1994), Galán and Pozo (2011), Yalçın and Bozkaya (2011), Karakaya et al. (2011), and Kaplan et al. (2013). The dense micritic calcite in calcretes reflects a relatively rapid and uniform precipitation and/or replacement (Tucker and Wright, 1990; Wright and Tucker, 1991; Nash and McLaren, 2003; Eren et al., 2008) from soil-derived water that has undergone some evaporation. At a more advanced stage of evaporation, palygorskite is evidenced

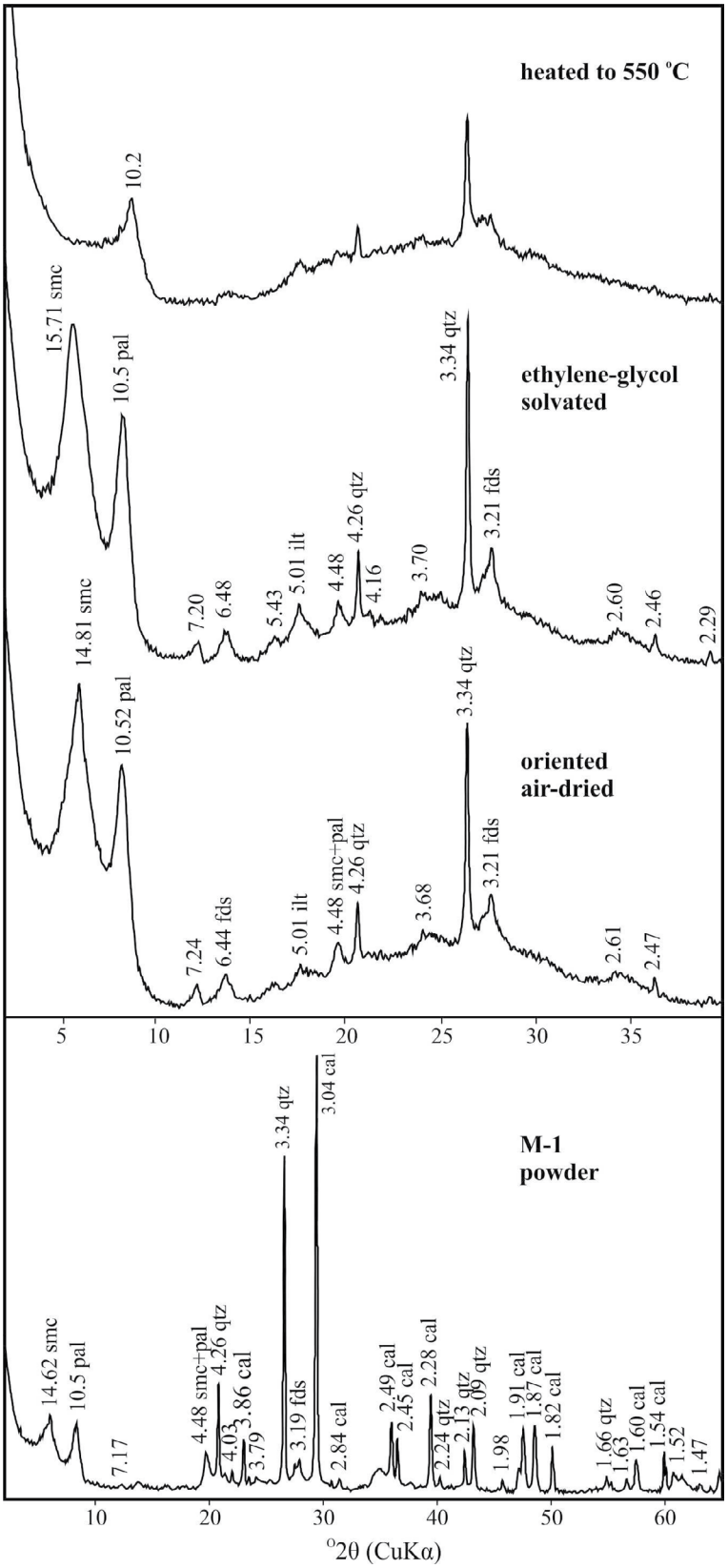

Figure 5. X-ray diffraction patterns for a palygorskite-smectite–dominated mudstone sample. pal: palygorskite, smc: smectite; ilt: illite, cal: calcite, qtz: quartz, fds: feldspar.

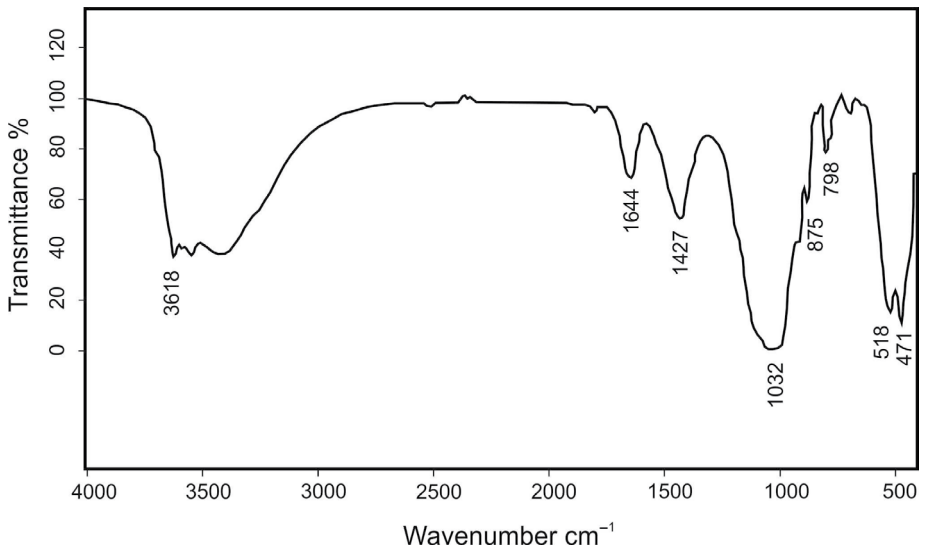

Figure 6. IR spectra of palygorskite-dominated sample.

by the presence of palygorskite fibres and fibre bundles extending from fine calcite crystals (Watts, 1980). Soil processes released isotopically light CO_2 into the meteoric percolating water, causing dissolution of calcium carbonate that later precipitated from supersaturated alkaline water as microcrystalline calcite and replaced the host-rocks/sediments from the same solution. Climate is a key factor in the formation of this mineral association. Aeolian dust is thought to be a major source of ions for calcrete formation (Goudie, 1973; Watts, 1980; Wright and Tucker, 1991). During dry periods, palygorskite formed from strongly evaporated percolating water after and/or during calcite precipitation under more alkaline conditions with high pH (ca. 8–11) and high Si and Mg and low Al and Fe ion activities (Singer and Norrish, 1974; Singer, 1979; Verrecchia and Le Coustumer, 1996; Colson et al., 1998; Akbulut and Kadir, 2003). Calcite precipitation from percolating waters at the early stages of calcrete formation led to a decrease in Ca, and a relative increase in the Al+Fe and Mg/Ca ratios, favouring the precipitation of palygorskite from an alkaline solution at a late stage (Hassouba and Shaw, 1980; Singer, 1989; Wang et al., 1993; Pimentel, 2002). The Si, Al+Fe, and Mg for palygorskite precipitation were derived possibly from smectite-dominated host-rock mudstone, because the smectite has a similar chemical composition to palygorskite (though with different element ratios; Table 2). The degradation of the Fe-bearing montmorillonite rather than saponitic smectite most likely caused the increase in the Al+Fe/Mg ratio, leading to precipitation of palygorskite in a pedogenic environment (formation within soil horizons) rather than sepiolite, which is more typically associated with precipitation from alkali-saline solutions in arid environments. This is also consistent with the fact that neither precipitation of sepiolite nor dolomitisation of calcite has occurred in these sediments (Akbulut and Kadir, 2003; Karakaya et al., 2004, 2011). The absence of palygorskite in the hardpan calcretes may be explained by the prevailing relatively more humid climatic conditions preventing the formation of palygorskite in this horizon prior to desiccation. Crystal morphologies of palygorskite are probably controlled by crystal surface, relief of crystal edges, and saturation. Encrusting and platy fan-like morphologies develop on the large crystal surfaces and may indicate precipitation from a very thin cover of water. The development of the wedge-shaped fibre bundles nucleating on the crystal edge reliefs is probably controlled by the morphology of the crystal edges. The morphology of the elongated palygorskite fibre bundles is consistent with precipitation from pendant water below the calcite crystal, supporting the presence of the vadose environment. Saturation and the length of the precipitation period may also control the size of palygorskite fibres (Gehring et al., 1995) together with the higher iron contents of the shorter fibres (Weaver and Pollard, 1973).

6. Conclusions

Palygorskite is closely associated with calcretes, suggesting a genetic relationship with calcrete formation in the Adana area. Palygorskite formation took place in a freshwater vadose environment in which it precipitated from highly alkaline percolating soil water rich in Si, Al, and Fe and low in Mg, and with a high pH, at an advanced stage of evaporation during calcrete formation. The authigenic character of the palygorskite is indicated by its delicate fibrous fabric.

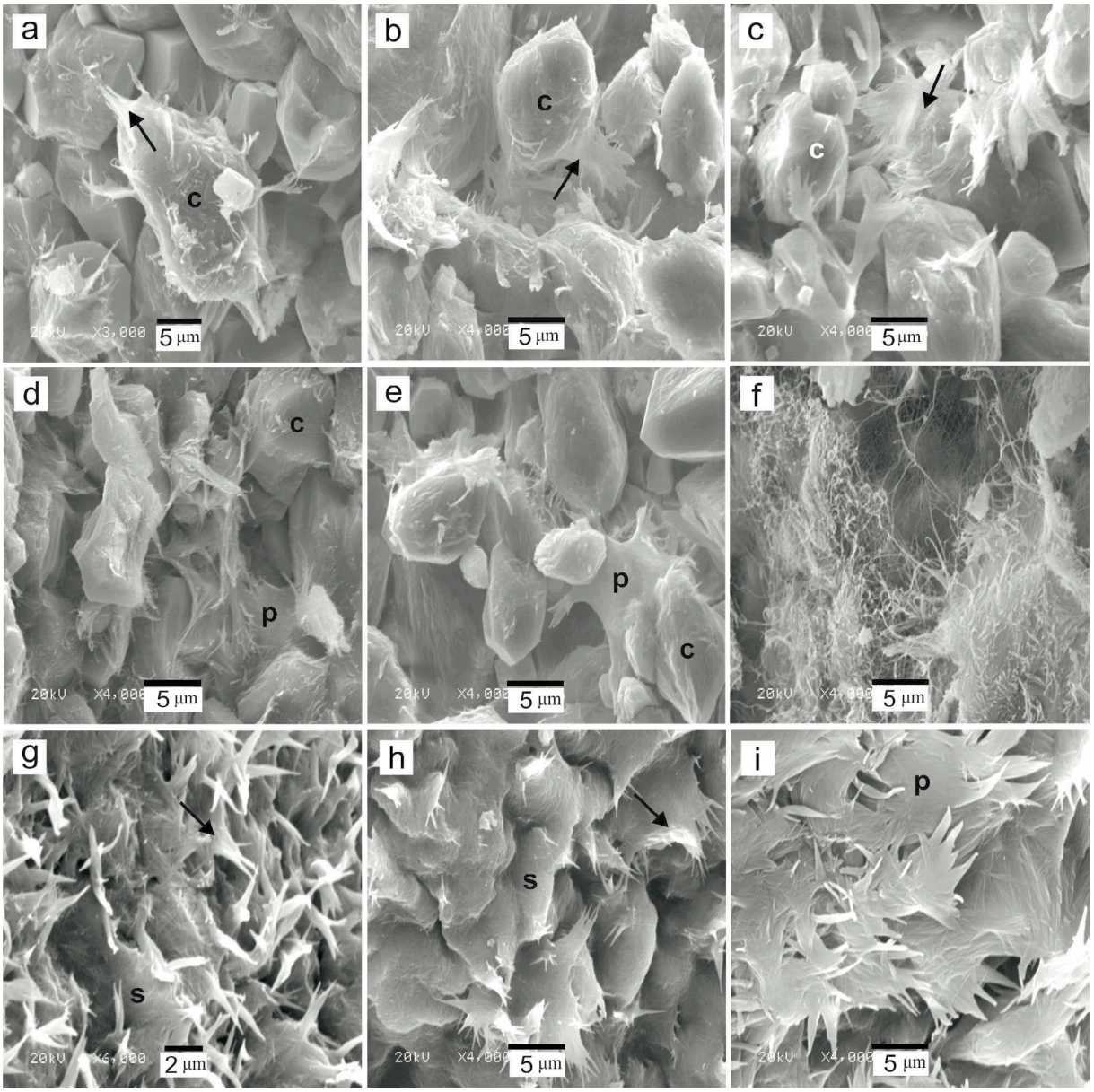

Figure 7. SEM images of palygorskite in calcretes **(a–e)** and host-rock mudstones **(f–i)**. **(a)** Palygorskite fibre bundles (arrow) extending from calcite crystal **(c)** to pore centre; **(b)** palygorskite sheet-like fibre bundle extending from calcite crystal **(c);** palygorskite fibre bundles (arrow) encrusting different inclined calcite crystal surfaces **(c)** likely precipitated from pendant water of the vadose zone; **(d, e)** pore-bridging palygorskite (p) fibre bundle extending from calcite (c) crystal indicating vadose environment; **(f)** interwoven palygorskite fibres extending from pore edge to pore centre; **(g, h)** wedge-shaped palygorskite fibre bundles (arrow) edging smectite (s) flakes; **(i)** platy fan-like palygorskite (p) fibre bundles.

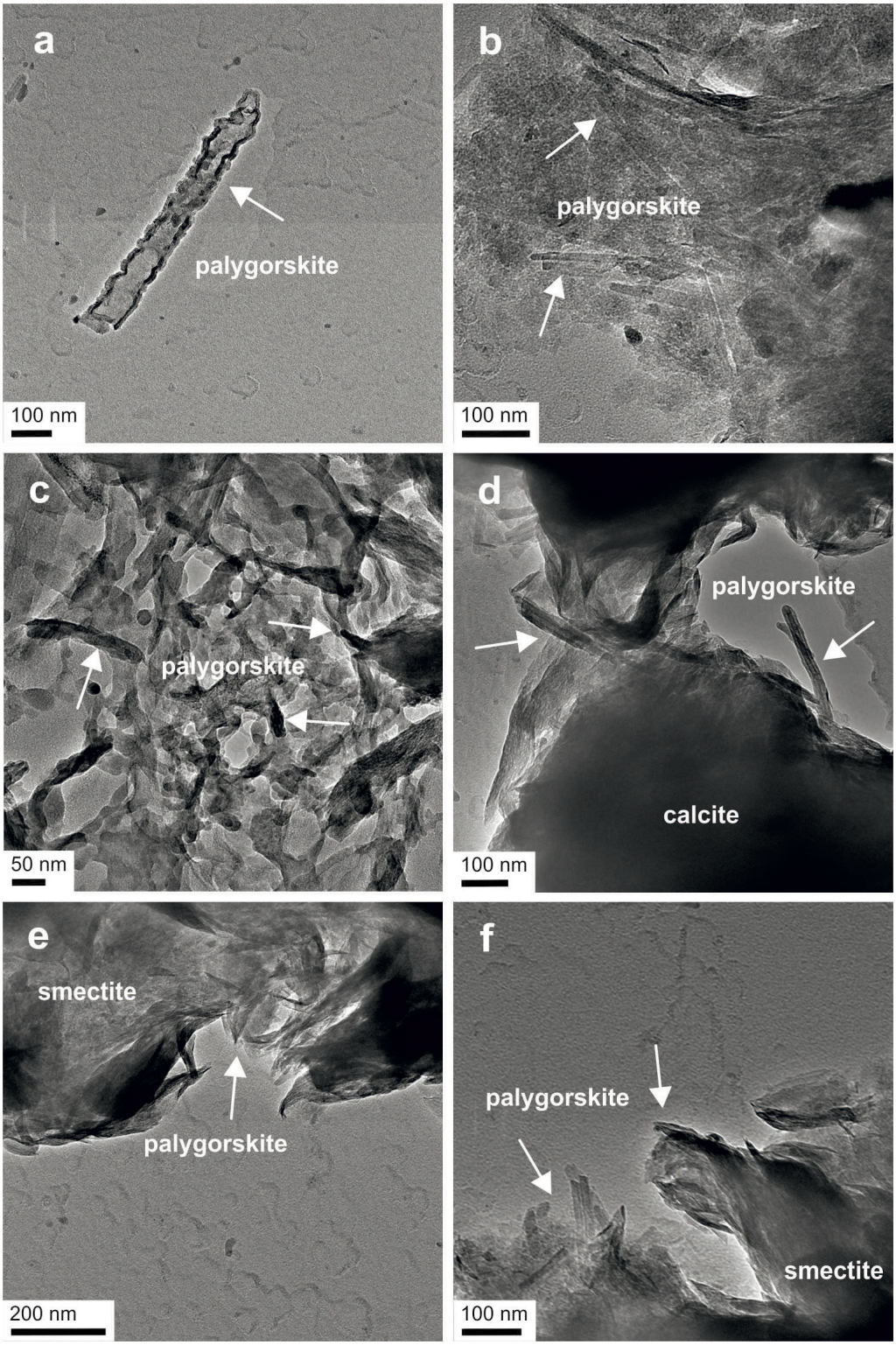

Figure 8. TEM images of: **(a)** individual palygorskite fibre (arrow); **(b)** palygorskite fibre bundles (arrow) extending from calcite crystal (c) to pore centre; **(c)** palygorskite fibre bundles showing a mesh-like structure and some fibres showing bending around the micropore indicating removal of impurities, **(d)** palygorskite fibres as a bridge or meniscus cement between altered calcite crystals and an individual palygorskite fibre extending from calcite crystal indicating vadose environment, **(e, f)** palygorskite fibre bundles with partially tapered and curled edge (arrow) extending from smectite crystal.

Table 2. Chemical compositions (wt.%) and structural formulas of palygorskite and smectite samples obtained from EDX analyses of single points. xt/xo= tetrahedral charge/octahedral charge ratio, CIA= chemical index of alteration.

Major oxides (wt.%)	Palygorskite YY-10	Smectite YY-10	Smectite YY-1	Smectite B-2	Smectite avg.
SiO_2	53.79	50.95	54.72	53.27	53.18
Al_2O_3	13.50	17.24	13.98	15.04	14.94
Fe_2O_3	5.03	8.36	7.63	6.49	6.88
MgO	7.65	2.83	3.58	3.85	4.48
CaO	0.56	1.63	1.71	1.83	1.43
K_2O	0.69	2.50	2.53	2.01	1.93
Sum	81.24	83.51	84.18	82.49	82.86
Si/Al	3.98	2.95	3.91	3.54	3.60
Tetrahedral					
Si	7.55	7.50	7.94	7.84	7.71
Al	0.45	0.50	0.06	0.16	0.29
S	8.00	8.00	8.00	8.00	8.00
Octahedral					
Al	1.78	2.49	2.33	2.45	2.26
Fe	0.53	0.93	0.83	0.72	0.75
Mg	1.60	0.62	0.77	0.84	0.96
S	3.91	4.04	3.93	4.01	3.97
Interlayer					
Ca	0.08	0.26	0.27	0.29	0.23
K	0.12	0.47	0.47	0.38	0.36
S	0.20	0.73	0.74	0.67	0.59
Tetrahedral charge	0.44	0.50	0.06	0.16	0.29
Octahedral charge	-0.13	0.50	0,98	0.80	0.60
Total charge	0.31	1.00	1.04	0.96	0.83
Interlayer charge	0.29	0.99	1.01	0.96	0.81
xt/xo	3.38	1.00	0.06	0.20	1.16
CIA	91.53	80.67	76.72	79.66	82.15

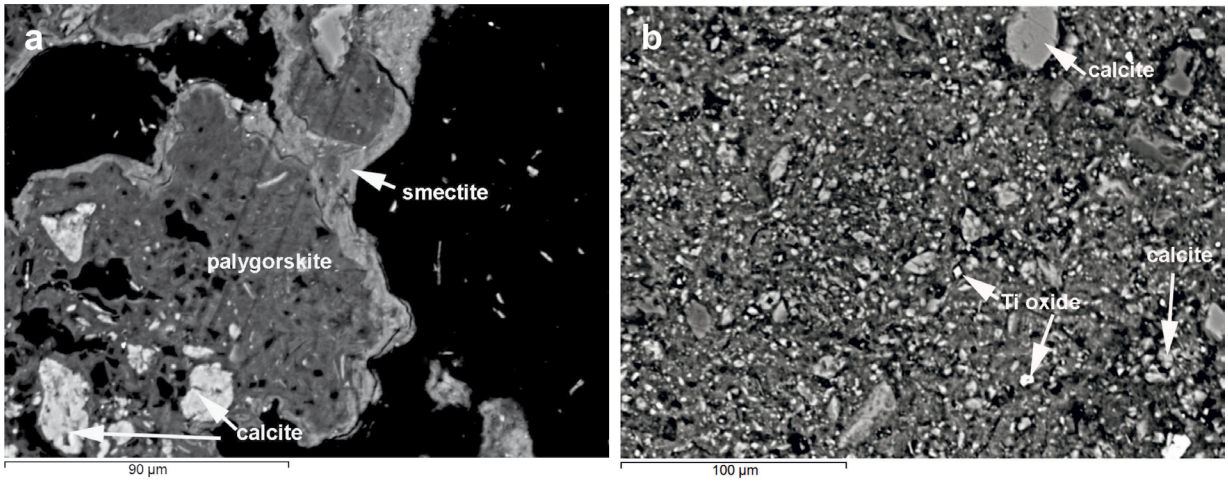

Figure 9. SEM images of polished-sections: **(a)** palygorskite aggregate with smectite rim/coating and associated calcite crystals, **(b)** Ti oxide and calcite minerals in the smectitic mudstone.

Acknowledgements
This study was supported financially by the Mersin University Research Fund under Project No. BAP-FBE JMB (MYK) 2009/3 DR. The authors are much indebted to the anonymous reviewers for their extremely careful and constructive reviews, which significantly improved the quality of the paper. We are also extremely grateful to Professor Muazzez Çelik Karakaya for her insightful editorial comments and suggestions. Miss Nergis Ünalgil is also thanked for assisting during the calculation of the structural formula of the clay minerals.

References

Akbulut A, Kadir S (2003). The geology and origin of sepiolite, palygorskite and saponite in Neogene lacustrine sediments of the Serinhisar-Acpayam basin, Denizli, SW Turkey. Clays Clay Miner 51: 279–292.

Allen BL, Hajek BF (1989). Mineral occurrence in soil environment. In: Dixon JB, Weed SB, editors. Minerals in Soil Environments. Soil Science Society of America Book Series 1. Madison, WI, USA: Soil Science Society of America, pp. 199–278.

Alonso-Zarza AM (1999). Initial stages of laminar calcrete formation by roots: examples from the Neogene of central Spain. Sediment Geol 126: 177–191.

Alonso-Zarza AM, Arenas C (2004). Cenozoic calcretes from the Teruel Graben, Spain: microstructure, stable isotope geochemistry and environmental significance. Sediment Geol 167: 91–108.

Altaner SP, Ylagan RF (1997). Comparison of structural models of mixed-layer illite/smectite and reaction mechanisms of smectite illitization. Clays Clay Miner 45: 517–533.

Atalay I (1996). Palaeosols as indicators of the climatic changes during Quaternary period in S Anatolia. J Arid Environ 32: 23–35.

Bajnoczi B, Horvath Z, Demeny A, Mindszenty A (2006). Stable isotope geochemistry of calcrete nodules and septarian concretions in a Quaternary 'red clay' paleovertisol from Hungary. Isot Environ Healt Stud 42: 335–350.

Botha GA, Hughes JC (1992). Pedogenic palygorkite and dolomite in a late Neogen sedimentary succession, Northwestern Transvaal, South Africa. Geoderma 53: 139–154.

Boutton TW (1991). Stable carbon isotope ratios of natural materials, II. Atmospheric, terrestrial, marine, and freshwater environments. In: Coleman C, Fry B, editors. Carbon Isotope Techniques. New York, NY, USA: Academic Press, pp. 173–186.

Bouza PJ, Simón M, Aquilar J, del Valle H, Rostagno M (2007). Fibrous-clay minerals formation and soil evolution in aridisols of NE Patagonia, Argentina. Geoderma 139: 38–50.

Brindley GW (1980). Quantitative X-ray analysis of clays. In: Brindley GW, Brown G, editors. Crystal Structures of Clay Minerals and Their X-ray Identification. Mineralogical Society Monograph 5. London, UK: Mineralogical Society, pp. 411–438.

Cerling TE (1984). The stable isotopic composition of modern soil carbonate and its relationship to climate. Earth Planet Sci Lett 71: 229–240.

Cerling TE (1992). Use of carbon isotopes in paleosols as indicator of the PCO_2 the paleoatmosphere. Global Biogeochem Cycles 6: 307–314.

Chahi A, Duplay J, Lucas J (1993). Analyses of palygorskite and associated clays from the Jbel Rhassoul (Morocco): chemical characteristics and origin of formation. Clays Clay Miner 41: 401–411.

Colson J, Cojan I, Thirty M (1998). A hydrogeological model for palygorskite formation in the Danian continental facies of the Provence Basin (France). Clay Miner 33: 333–347.

Dudek T, Cuadros J, Fiore S (2006). Interstratified kaolinite-smectite: Nature of the layers and mechanism of smectite kaolinization. Am Mineral 91: 159–170.

Elprince AM, Mashhady AS, Aba-Husayn MM (1979). The occurrence of pedogenic palygorskite (attapulgate) in Saudi Arabia. Soil Sci 128: 211–218.

Eren M (2011). Stable isotope geochemistry of Quaternary calcretes in the Mersin area, southern Turkey - a comparison and implications for their origin. Chem Erde 71: 31–37.

Eren M, Kadir S, Hatipoğlu Z, Gül M (2004). Caliche Development in Mersin Area. TÜBİTAK Project No. 102Y036. Ankara, Turkey: TÜBİTAK (in Turkish with English abstract).

Eren M, Kadir S, Hatipoğlu Z, Gül M (2008). Quaternary calcrete development in the Mersin area, southern Turkey. Turkish J Earth Sci 17: 763–784.

Eren M, Kaplan MY, Kadir S (2007). Petrography, geochemistry and origin of Lower Jurassic dolomites in the Aydıncık area, Mersin, southern Turkey. Turkish J Earth Sci 16: 339–362.

Farmer VC (1974). Infrared spectra of minerals. In: Farmer VC, editor. Monograph 4. London, UK: Mineralogical Society, pp. 331–363.

Foster MD (1953). Geochemical studies of clay minerals. II Relation between ionic substitution and swelling in montmorillonite. Am Mineral 38: 994–1006.

Frost RL, Locos OB, Ruan J, Kloprogge JT (2001). Nearinfrared and mid-infrared spectroscopic study of sepiolites and palygorskites. Vib Spectrosc 27: 1–3.

Galán E, Pozo M (2011). Palygorskite and sepiolite deposits in continental environments. Description, genetic patterns and sedimentary settings. In: Galán E, Singer E, editors. Developments in Palygorskite-Sepiolite Research. A New Outlook on these Nanomaterials. Developments in Clay Science, Vol. 3. Amsterdam, the Netherlands: Elsevier, pp. 125–173.

Garcia-Romero E, Suárez M (2010). On the chemical composition of sepiolite and palygorskite. Clays Clay Miner 58: 1–20.

Gong SY, Mii HS, Wei KY, Horng CS, You CF, Huang FW, Chi WR, Yui TZ, Torng PK, Huang ST et al. (2005). Dry climate near the Western Pacific Warm Pool: Pleistocene caliches of the Nansha Islands, South China Sea. Palaeogeogr Palaeoclimatol Palaeoecol 226: 205–213.

Goudie AS (1973). Duricrusts in Tropical Landscapes. Oxford, UK: Clarendon Press.

Gürbüz K (1999). Regional implications of structural and eustatic controls in the evolution of submarine fans: an example from the Miocene Adana Basin, southern Turkey. Geol Mag 136: 311–319.

Hassouba H, Shaw HF (1980). The occurrence of palygorskite in the Quaternary sediments of the coastal plain of North-west Egypt. Clay Miner 15: 77–83.

Hillier S, Pharande AL (2008). Contemporary pedogenic formation of palygorskite in irrigation-induced, saline-sodic, shrink-swell soils of Maharashtra India. Clays Clay Miner 56: 531–548.

Hower J, Eslinger E, Hower M, Perry E (1976). The mechanism of burial diagenetic reactions in argillaceous sediments: 1. Mineralogical and chemical evidence. Geol Soc Am Bull 87: 725–737.

Inglès M, Anadón P (1991). Relationship of clay minerals to depositional environment in the non-marine Eocene Pontils Group, SE Ebro basin (Spain). J Sediment Petrol 61: 926–939.

Inoue A, Meunier A, Beaufort D (2004) Illite-smectite mixed-layer minerals in felsic volcaniclastic rocks from drill cores, Kakkonda, Japan. Clays Clay Miner 52: 66–84.

James NP, Choquette PW (1984). Diagenesis 9. Limestones - The meteoric diagenetic environment. Geosci Can 11: 161–194.

Jimenez De Cisneros C, Molina JM, Nieto LM, Ruiz-Ortiz PA, Vera JA (1993). Calcretes from a palaeosinkhole in Jurassic palaeokarst (Subbetic, southern Spain). Sediment Geol 87: 13–24.

Kadir S, Eren M (2008). The occurrence and genesis of clay minerals associated with Quaternary caliches in the Mersin area, southern Turkey. Clays Clay Miner 56: 244–258.

Kadir S, Eren M, Atabey E (2010). Dolocretes and associated palygorskite occurrences in siliciclastic red mudstones of the Sariyer formation (Middle Miocene), southeastern side of the Çanakkale strait, Turkey. Clays Clay Miner 58: 205–219.

Kadir S, Eren M, Külah T, Önalgil N, Cesur M, Gürel A (2014). Genesis of Late Miocene-Pliocene lacustrine palygorskite and calcretes from Kırşehir, central Anatolia, Turkey. Clay Miner 49: 433–454.

Kaplan MY, Eren M, Kadir S, Kapur S (2013). Mineralogical, geochemical and isotopic characteristics of Quaternary calcretes in the Adana region, southern Turkey: Implications on their origin. Catena 101: 164–177.

Kapur S, Çavuşgil VS, Fitzpatrick EA (1987). Soil-calcrete (caliche) relationship on a Quaternary surface of the Cukurova Region, Adana (Turkey). In: Federoff N, Bresson LM, Courty MA, editors. Soil Micromorphology. Paris, France: Association Française pour L'Etude du sol, pp. 597–603.

Kapur S, Çavuşgil VS, Şenol M, Gürel N, Fitzpatrick E A (1990). Geomorphology and pedogenic evolution of Quaternary calcretes in the northern Adana Basin of southern Turkey. Z Geomorphol 34: 49–59.

Kapur S, Saydam C, Akça E, Çavuşgil VS, Karaman C, Atalay I, Özsoy T (2000). Carbonate pools in soil of the Mediterranean: A case study from Anatolia. In: Lal R, Kimble JM, Eswaran H, Stewart BA, editors. Global Climate Change and Pedogenic Carbonates. Boca Raton, FL, USA: Lewis Publishers, pp. 187–212.

Kapur S, Yaman S, Gokçen SL, Yetiş C (1993). Soil stratigraphy and Quaternary caliche in the Misis area of the Adana Basin, southern Turkey. Catena 20: 431–445.

Karakaya N, Karakaya MÇ, Temel A (2011). Mineralogical and geochemical characteristics and genesis of the sepiolite deposits at Polatlı Basin (Ankara, Turkey). Clays Clay Miner 59: 286–314.

Karakaya N, Karakaya MÇ, Temel A, Küpeli Ş, Tunoğlu C (2004). Mineralogical and chemical characterization of the sepiolite occurrences at Karapınar (Konya Basin, Turkey). Clays Clay Miner 52: 495–510.

Krekeler MPS, Hammerly E, Rakovan J, Guggenheim S (2005). Microscopy studies of the palygorskite-to-smectite transformation. Clays Clay Miner 53: 92–99.

Küçükuysal C, Kapur S (2014). Mineralogical, geochemical and micromorphological evaluation of the Plio-Quaternary paleosols and calcretes from Karahamzalı, Ankara (Central Turkey). Geol Carpath 65: 241–253.

Millot G (1970). Geology of Clays. New York, NY, USA: Springer-Verlag.

Moore DM, Reynolds RC (1989). X-ray diffraction and the identification and analysis of clay minerals. Oxford, UK: Oxford University Press.

Nash DJ, McLaren SJ (2003). Kalahari valley calcretes: their nature, origins, and environmental significance. Quatern Int 111: 3–22.

Özer AM, Wieser A, Göksu HY, Müller P, Regulla DF, Erol O (1989). ESR and TL age determination of caliche nodules. Int J Radiat Appl Instrum A 40: 1159–1162.

Pimentel NLV (2002). Pedogenic and early diagenetic processes in Palaeogene alluvial fan and lacustrine deposits from the Sado Basin (S Portual). Sediment Geol 148: 123–138.

Purvis K, Wright VP (1991). Calcretes related to phreatophytic vegetation from the Middle Triassic Otter Sandstone of South West England. Sedimentology 38: 539–551.

Rodas M, Luque FJ, Mas R, Garzon MG (1994) Calcretes, palycretes and silcretes in the Paleogene detrital sediments of the Dueo and Tajo Basins, central Spain. Clay Miner 29: 273–285.

Rogers LER, Martin AE, Norrish K (1954). The occurrence of palygorskite near Ipswich, Queensland. Mineral Mag 30: 534–540.

Sánchez C, Galán E (1995) An approach to the genesis of palygorskite in a Neogene-Quaternary continental basin using principal factor analysis. Clay Miner 30: 225–238.

Shaaban MN (2004). Diagenesis of the lower Eocene Thebes Formation, Gebel Rewagen area, Eastern Desert, Egypt. Sediment Geol 165: 53–65.

Singer A (1979). Palygorskite in sediments: detrital, diagenetic, or neoformed-a critical review. Geol Rundsch 68: 996–1008.

Singer A (1989). Palygorskite and sepiolite group minerals. In: Dixon JB, Weed SB, editors. Minerals in Soil Environments. Soil Science Society of America Book Series 1. Madison, WI, USA: Soil Science Society of America, pp. 829–872.

Singer A, Norrish K (1974). Pedogenic palygorskite occurrences in Australia. Am Mineral 59: 508–517.

Strong GE, Giles JRA, Wright VP (1992). A Holocene calcrete from North Yorkshire, England: implications for interpreting palaeoclimates using calcretes. Sedimentology 39: 333–347.

Suárez M, García-Romero E (2006). FTIR spectroscopy study of palygorskite: Influence of the composition of the octahedral sheet. Appl Clay Sci 31: 154–163.

Suárez M, Robert M, Elsass F, Martin Pozas JM (1994). Evidence of a precursor in the neoformation of palygorskite- new data by analytical electron microscopy. Clay Miner 29: 255–264.

Tucker ME, Wright VP (1990). Carbonate Sedimentology. Oxford, UK: Blackwell Scientific Publications.

Verrecchia EP, Le Coustumer MN (1996). Occurrence and genesis of palygorskite and associated clay minerals in a Pleistocene calcrete complex, Sde Bowuer, Negev Desert, Israel. Clay Miner 31: 183–202.

Wang MK, Tseng PC, Chang SS, Ray DT, Shau YH, Shen YW, Chen RC, Chiang PN (2009). Origin and mineralogy of sepiolite and palygorskite from the Tuluanshan formation, eastern Taiwan. Clays Clay Miner 57: 521–530.

Wang Y, Nahon D, Merino E (1993). Geochemistry and dynamics of calcrete genesis in semi-arid regions. Chem Geol 107: 349–351.

Watts NL (1980). Quaternary pedogenic calcretes from the Kalahari (southern Africa): mineralogy, genesis and diagenesis. Sedimentology 27: 661–686.

Weaver CE, Pollard LD (1973) The Chemistry of Clay Minerals. New York, NY, USA: Elsevier.

Wright VP, Tucker ME (1991). Calcretes. Oxford, UK: Blackwell Scientific Publications.

Yalçın H, Bozkaya Ö (2011). Sepiolite-palygorskite occurrences in Turkey. In: Galan E, Singer A, editors. Developments in Clay Science, Vol. 3. Amsterdam, the Netherlands, pp. 175–200.

Yalçın MN, Görür N (1983). Sedimentological evolution of the Adana Basin. In: Tekeli O, Göncüoğlu MC, editors. Geology of the Taurus Belt. Proceedings of International Tauride Symposium. Ankara, Turkey: Mineral Research and Exploration Institute of Turkey (MTA), pp. 165–172.

Yeniyol M (2012). Geology and mineralogy of a sepiolite-palygorskite occurrence from SW Eskişehir (Turkey). Clay Miner 47: 93–104.

Yetiş C (1988). Reorganization of the Tertiary stratigraphy in the Adana Basin, southern Turkey. Stratigr Newsl 20: 43–58.

Yetiş C, Kelling G, Gökçen SL, Baroz F (1995). A revised stratigraphic framework for later Cenozoic sequences in the northeastern Mediterranean region. Geol Rundsch 84: 794–812.

Yılmaz K (1999). The genesis of smectite and palygorskite on Harran Plain's soil series. Tr J Agric For 23: 636–642.